Dissertation

Imaging of Single Barium Atoms in Solid Xenon for the nEXO Neutrinoless Double Beta Decay Experiment

Submitted by

Timothy Walton

Department of Physics

In partial fulfillment of the requirements

For the Degree of Doctor of Philosophy

Colorado State University

Fort Collins, Colorado

Fall 2015

Doctoral Committee:

Advisor: William M. Fairbank, Jr.

Robert Wilson
Bruce Berger
Alan Van Orden

Abstract

The nEXO experiment is designed to search for zero-neutrino double beta decay of the isotope ^{136}Xe, in order to better understand the nature of neutrinos. Since the daughter of this decay is barium (^{136}Ba), detecting the presence of ^{136}Ba at a decay site (called "barium tagging") provides an additional discriminator to reject backgrounds in the search for this decay. This would involve detecting a single barium ion from within a macroscopic volume of liquid xenon. One proposed barium tagging method is to trap the barium ion in solid xenon (SXe) at the end of a cold probe, and then detect the ion by its fluorescence in the solid xenon. William M. Fairbank Jr.'s group at Colorado State University has been working toward this goal with steady success for some time. In this thesis, I demonstrate successful detection of neutral Ba in SXe down to the single atom level, after deposition from vacuum.

Acknowledgements

Bill, Chris for all the help in the lab and building things, Shon and Brian for creating the system and training me (Shon) and for the preliminary results, Adam, Cesar, Kendy.

If you want the Leif thing, uncomment it in csuthesis.cls. It says something like "this dissertation is typeset in ... designed by Leif Anderson.

Jamie and LEW, and other fam.

Table of Contents

Abstract ii

Acknowledgements iii

Chapter 1. Introduction 1

1.1. Neutrinos 2

1.2. Enriched Xenon Observatory 7

Chapter 2. Theory 19

2.1. Ba/Ba^+ Spectroscopy in Vacuum 19

2.2. Matrix Isolation Spectroscopy 20

Chapter 3. Apparatus 23

3.1. Ion Beam 23

3.2. Ba Getter Source 27

3.3. Solid Xenon Matrix Deposition 28

Chapter 4. Results 29

4.1. Fluorescence of Ba in SXe 29

4.2. Bleaching 30

4.3. Imaging 30

Chapter 5. Conclusions 31

5.1. Future Steps 31

Bibliography 32

CHAPTER 1

Introduction

Neutrinos have been at the forefront of discovery since their prediction by W. Pauli, who proposed in 1930 the existence of a neutral, unobserved particle to explain the apparent violation of energy conservation in beta decay [1]. He admitted that neutrinos (then deemed "neutrons" – what we now know as neutrons had not been discovered yet either) should be difficult to observe experimentally, but also that it seemed unlikely that they would never have been noticed before. As it turns out, they are much more difficult to observe than he predicted; they will not be noticed without extreme experimental techniques.

A theory formulated in 1933 by E. Fermi for beta decay [2], including the neutrino, would be the beginnings of weak theory, and the development of the very successful Standard Model of particle physics. But neutrinos continued to challenge theory with the discovery of non-zero neutrino mass, and they remain at the forefront of our exploration of the universe.

The possibility that neutrinos are Majorana particles makes the search for neutrinoless double beta decay very important for the further development of particle theory. Majorana formulation can describe the origin of neutrino mass, and possibly explain why the mass is very small via the Seesaw Mechanism [ref]. Observation of neutrinoless double beta decay would simultaneously demonstrate that neutrinos are Majorana particles, as well as give a measurement of the absolute mass itself [ref? this is said later too].

To motivate barium tagging, this chapter outlines the current theory for neutrinos, and then describes the neutrinoless double beta decay experiments EXO-200 and nEXO.

1.1. Neutrinos

Neutrinos are chargeless leptons which only interact via the weak force (and gravity). There are three known "flavors" of neutrinos, each corresponding to one of the three known leptons: ν_e, ν_μ, and ν_τ. These are the eigenstates in the basis of the weak force, so they are the states in which a neutrino will interact via the weak force.

1.1.1. Neutrino Oscillation and Mass.

The postulate that neutrinos have an energy basis which is different from the flavor basis predicts the phenomenon of oscillation – that the time evolution of an initially pure flavor state (as a neutrino will be produced) will result in a time-dependent probability of measuring the other two flavors as well.

The very small mass of a neutrino (assumed zero in the SM), specifically relative to its momentum, lets one write its Hamiltonian in terms of mass squared differences $\Delta m^2_{ij} = m^2_i - m^2_j$, where i,j = 1,2,3, referring to what we then call mass states. The mass basis is really the energy basis with the small mass approximation, along with dropping some constant terms in the Hamiltonian (which do not affect time evolution). Writing the time evolution in terms of mass squared differences means that neutrino oscillation experiments can produce measurements of these differences. In fact, the discovery of neutrino oscillation was the first (and only, so far) demonstration that neutrinos have a non-zero mass. Without neutrino mass (particularly without differences between the masses of the mass states), neutrinos would not oscillate.

Neutrino oscillation experiments also provide measurements on the amount of mixing between the flavor basis and the mass basis. We define the mixing between them by a rotation in terms of three mixing angles, θ_{12}, θ_{23}, and θ_{13}. Transformation between the

flavor and mass bases is done with the following unitary matrix, called the Pontecorvo–Maki-Nakagawa-Sakata (PMNS) matrix:

$$
\begin{aligned}
U &= \begin{pmatrix} 1 & 0 & 0 \\ 0 & c_{23} & s_{23} \\ 0 & -s_{23} & c_{23} \end{pmatrix} \begin{pmatrix} c_{13} & 0 & s_{13}e^{-i\delta} \\ 0 & 1 & 0 \\ -s_{13}e^{i\delta} & 0 & c_{13} \end{pmatrix} \begin{pmatrix} c_{12} & s_{12} & 0 \\ -s_{12} & c_{12} & 0 \\ 0 & 0 & 1 \end{pmatrix} \begin{pmatrix} 1 & 0 & 0 \\ 0 & e^{i\alpha_1/2} & 0 \\ 0 & 0 & e^{i\alpha_2/2} \end{pmatrix} \\
&= \begin{pmatrix} c_{12}c_{13} & s_{12}c_{13} & s_{13}e^{-i\delta} \\ -s_{12}c_{23} - c_{12}s_{23}s_{13}e^{i\delta} & c_{12}c_{23} - s_{12}s_{23}s_{13}e^{i\delta} & s_{23}c_{13} \\ s_{12}s_{23} - c_{12}c_{23}s_{13}e^{i\delta} & -c_{12}s_{23} - s_{12}c_{23}s_{13}e^{i\delta} & c_{23}c_{13} \end{pmatrix} \begin{pmatrix} 1 & 0 & 0 \\ 0 & e^{i\alpha_1/2} & 0 \\ 0 & 0 & e^{i\alpha_2/2} \end{pmatrix}
\end{aligned} \tag{1}
$$

where $c_{ij} = \cos\theta_{ij}$ and $s_{ij} = \sin\theta_{ij}$. δ is a phase factor related to lepton CP violation, and α_i are Majorana phases.

Studying oscillations of neutrinos from different kinds of sources, with different energies and path lengths, can isolate sensitivities to the different parameters. For example, the study of solar neutrinos (neutrinos emanating from nuclear fusion reactions in the core of the sun) provides sensitivity to θ_{12} and Δm^2_{12}. The oscillation parameters so far measured shown in Table 1.1:

TABLE 1.1. Best-fit values for neutrino oscillation parameters, from a global fit to oscillation experiment data. [talk about definition of atsmopheric thing relying on hierarchy][3]

Parameter	Measurement ($\pm 1\sigma$)
Δm^2_{12}	$7.54^{+0.26}_{-0.22}$ 10^{-5} eV^2
$\lvert\Delta m^2\rvert$	2.43 $\pm$ 0.06 (2.38 $\pm$ 0.06) 10^{-3} eV^2
$\sin^2\theta_{12}$	0.308 $\pm$ 0.017
$\sin^2\theta_{23}$	$4.37^{+0.033}_{-0.023}$ $(4.55^{+0.039}_{-0.031})$
$\sin^2\theta_{13}$	$0.0234^{+0.0020}_{-0.0019}$ $(0.0240^{+0.0019}_{-0.0022})$
δ/π (2σ range)	$1.39^{+0.38}_{-0.27}$ $(1.31^{+0.29}_{-0.33})$

[talk about this as the "atmospheric" one] Note that only the absolute value of $\Delta m^2_{31(2?)}$ is known. As a consequence, there are two possibilities for the hierarchy of the three neutrino masses. These are called the Normal and Inverted Hierarchies, as shown in Fig. 1.1.

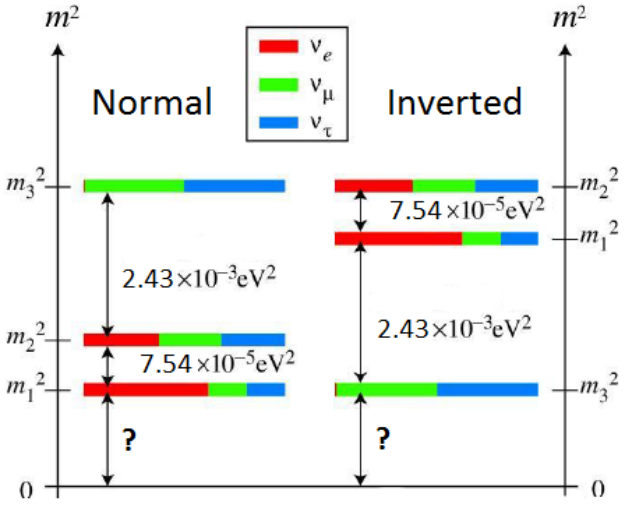

FIGURE 1.1. The two possible hierarchies of neutrino masses. The colors depict the mixing between the mass and flavor bases. [ref]

The correct mass hierarchy remains unknown, but next-generation neutrino experiments, possibly including nEXO, will be able to discern this.

Neutrino oscillation demonstrates that neutrinos have non-zero mass, and though oscillation experiments can measure the mass squared differences, we still do not have a measurement of the absolute masses of the three neutrinos.

Neutrinoless double beta decay experiments like EXO-200 search for specifically the Majorana neutrino mass (i.e., neutrino mass if neutrinos are indeed Majorana particles). Cosmology can put limits on the sum of the three neutrino masses, the current limit of which is [???] [ref planck or somthing else]. The KATRIN experiment aims to measure the neutrino mass by accurately observing the spectrum of tritium beta decay near the Q-value [ref KATRIN].

Neutrino oscillation and non-zero neutrino mass are physics beyond the Standard Model (SM) of particle physics, and though much has been discovered through oscillation experiments, there is much yet to learn about neutrinos. Since they are chargeless, they may be Majorana particles, and their small mass could be explained by the See-saw Mechanism [ref]. Majorana particles are their own anti-particle, and this, along with the discovery that neutrinos have mass, allows for a unique test of the Majorana (vs. Dirac) nature of neutrinos: neutrinoless double beta decay.

1.1.2. Neutrinoless Double Beta Decay. Double beta decay is the simultaneous emission of two electrons from a nucleus. Two-neutrino double beta decay, shown in Fig. 1.2(left), is allowed by the Standard Model and has been observed in several isotopes which are listed in Table 1.2. Similar to beta decay, a neutrino accompanies each electron in this decay, broadening the spectrum of the summed electron energy. This is a second-order process, making it a rare decay, and requiring low backgrounds to measure.

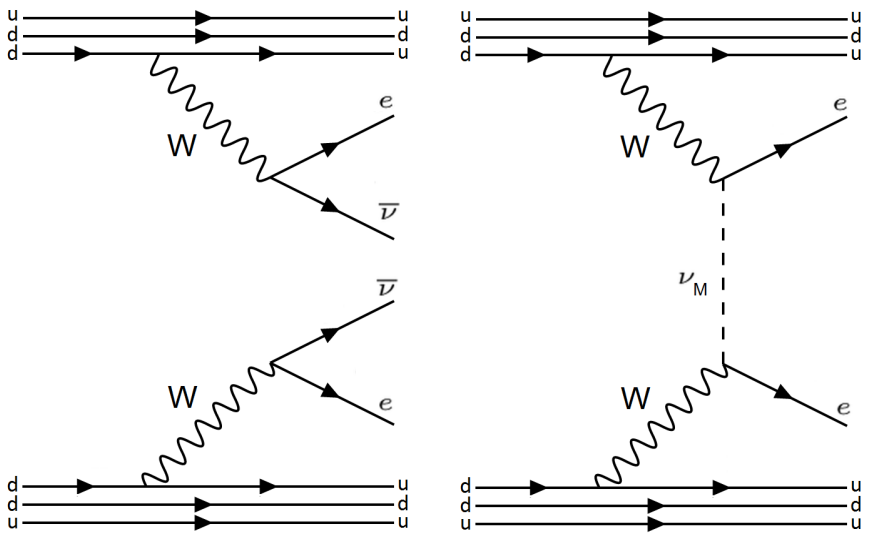

Figure 1.2. Two-neutrino (left) and Neutrinoless (right) double beta decay.

Neutrinoless double beta decay, shown in Fig. 1.2(right), is a postulated mode of double beta decay. In this case, the neutrino is exchanged as a virtual particle (which would require that it is a Majorana particle), and there are no neutrinos in the final products. If discovered, not only would neutrinos be determined Majorana particles, but their absolute mass could also be measured in the form of an effective electron neutrino mass, since the rate of neutrinoless double beta decay will depend on the absolute neutrino mass as shown in Eqn. 2:

$$T_{1/2}^{0\nu} = (G^{0\nu}(Q,Z)|M^{0\nu}|^2 \langle m_\nu \rangle^2)^{-1} \tag{2}$$

where $T_{1/2}^{0\nu}$ is the $0\nu\beta\beta$ half-life, $G^{0\nu}$ is a known phase space factor, and $M^{0\nu}$ is a model-dependent nuclear matrix element. The effective electron neutrino mass $\langle m_\nu \rangle$ is the expectation value of the mass for a pure electron neutrino:

$$\langle m_\nu \rangle = \sum_i U_{ei}^2 m_i. \tag{3}$$

The sum of the energies of the emitted electrons in double beta decay will serve as the distinction between the two-neutrino and zero-neutrino modes, shown in Fig. 1.3. In the two-neutrino mode, the total decay energy is shared probabilistically between the electrons and the neutrinos (the nucleus recoil energy is negligible), resulting in a broad distribution in the summed electron energy. (Recall the similarly broad electron energy in single beta decay, which ultimately led to discovery of the neutrino involved.) But in the zero-neutrino mode, all of the decay energy is carried away by the two electrons, resulting in only a single allowed

value for the summed electron energy – a peak in the summed electron energy spectrum at the Q-value.

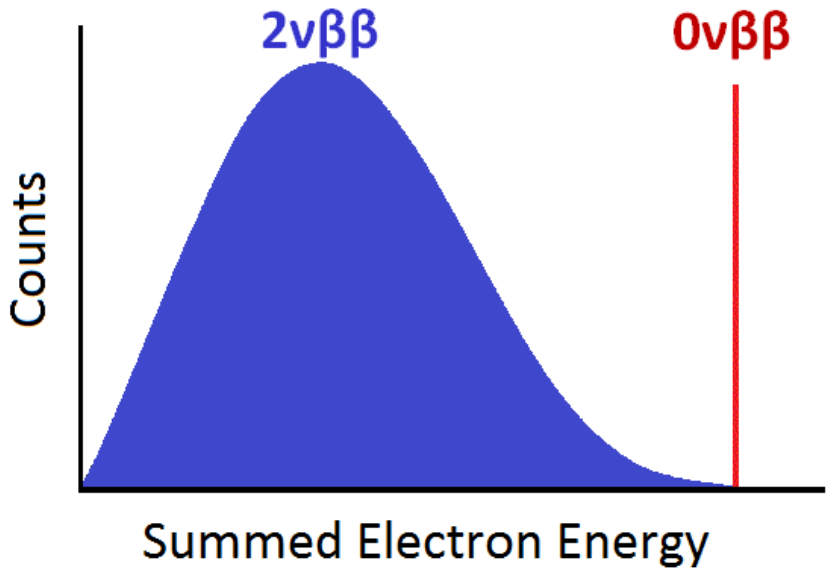

FIGURE 1.3. Conceptual two-neutrino (blue) and zero-neutrino (red) double beta decay spectra.

TABLE 1.2. $2\nu\beta\beta$ half-lives measured for various isotopes.

Isotope	Experiment	$T^{2\nu}_{1/2}$
^{136}Xe	EXO-200	2.
...	...	...

The rarity of double beta decay (see the very long half lives in Table 1.2) requires very low backgrounds, especially around the Q-value for the $0\nu\beta\beta$ search. The next sections describe EXO-200 and it's next-generation successor, nEXO.

1.2. Enriched Xenon Observatory

The Enriched Xenon Observatory (EXO) is a set of two experiments, each a LXe time projection chamber (TPC) designed to study the double beta decay of the isotope ^{136}Xe, and ultimately to search for the zero-neutrino mode. There are several advantages to a LXe detector. Xe is extremely transparent, and scintillates at [around?] [xxx] nm, which is

[efficiently collected by [type that the APDs are]] [reference]; so the Xe acts as a detection medium in addition to being the source of the double beta decay [reference? I didn't make up that kind of sentence]. Xe can be continuously purified to maintain large electron lifetimes in the LXe. Also, the ratio between observed scintillation light and remaining ionized electrons (drifted from the decay site by the TPC's electric field) exhibits a well-known microscopic anti-correlation [ref.], the understanding of which improves the energy resolution of the detector. Finally, a LXe TPC approach offers the opportunity, [fairly] unique in double beta decay, to reach in and identify, or "tag", the daughter Ba^{++} at the site of the double beta decay event, which would provide a background-free identification of neutrinoless double beta decay. Barium tagging is the focus of our group at CSU and is the subject of this thesis.

The following sections decribe the EXO-200 experiment, as well as nEXO, the next-generation tonne-scale LXe TPC which is now in the design stages. EXO-200 does not have barium tagging implemented, but it is hoped that nEXO will.

1.2.1. EXO-200. EXO-200 has been operational since 2011. It is a LXe TPC designed to probe Majorana neutrino masses down to around 100 meV [EXO instrum. paper part I], and is located about half a mile underground in the Waste Isolation Pilot Plant (WIPP) near Carlsbad, NM. This mine is in a salt basin, which contains lower levels of Uranium and Thorium than a typical mine in rock, making it more ideal for a low-background experiment. WIPP's main purpose is to permanently store transuranic nuclear waste, which is stored at the other end of the mine and is not an issue for EXO-200.

A schematic of the TPC in the class 100 cleanroom is shown in Fig. 1.4. Several layers of lead wall surround the copper cryostat, which is filled with hydro-fluoro-ethylwhatever

(HFE), a cryogenic fluid which keeps the TPC cooled to LXe temperatures, as well as aids in shielding. The copper material of the cryostat and TPC is [purified or something?], and is kept as thin as possible to minimize backgrounds. Scintillating panels on the outside of the cleanroom provide muon veto.

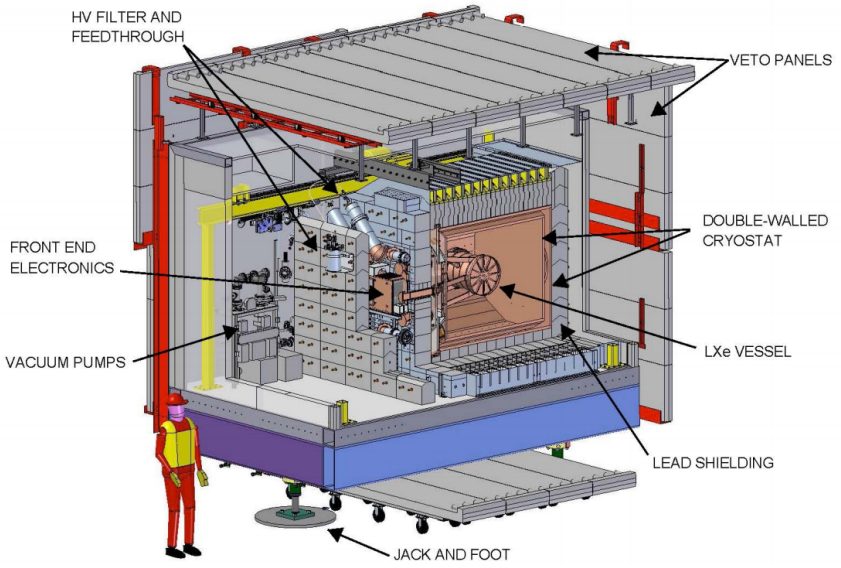

FIGURE 1.4. Drawing of cleanroom laboratory in the WIPP drift. **Find better-rez pic.**

Fig. 1.5 shows the EXO-200 detector. It is actually two face-to-face TPCs which share a cathode. The detection planes are a combination of ionized charge induction/collection wires and avalanche photodiodes which detect scintillation light.

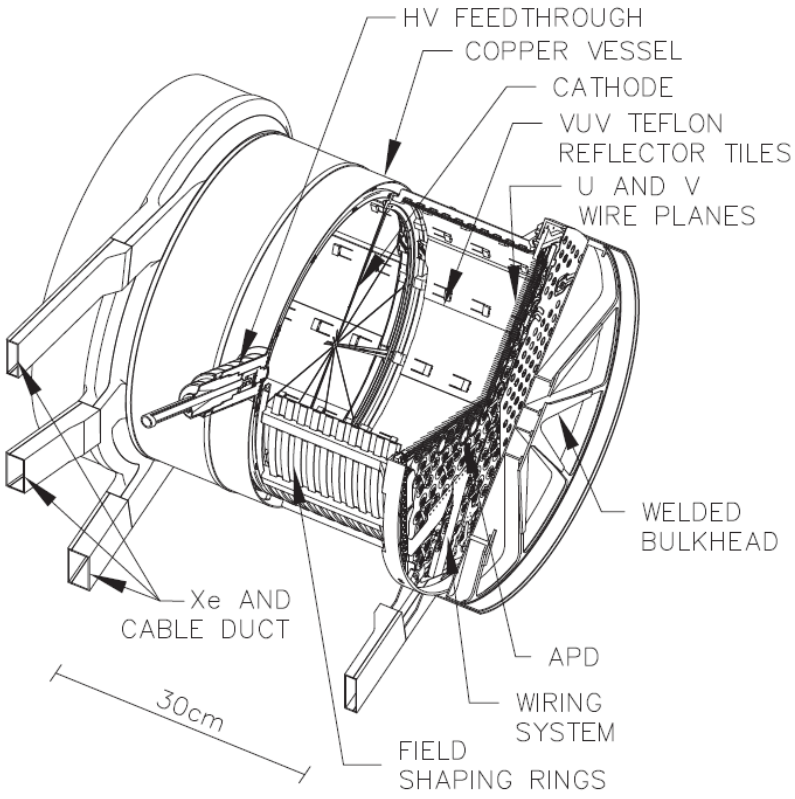

FIGURE 1.5. EXO-200 TPC diagram. [ref 2ν long paper]

A photograph of the detection plane is shown in Fig. 1.6, and a schematic of event detection is shown in Fig. 1.7. When a double beta decay event occurs in the LXe, the energetic electrons ionize many surrounding Xe atoms. Some electrons very quickly recombine, emitting scintillation light which is collected by the APDs. This is part of the energy collection, and also provides a time stamp for the event.

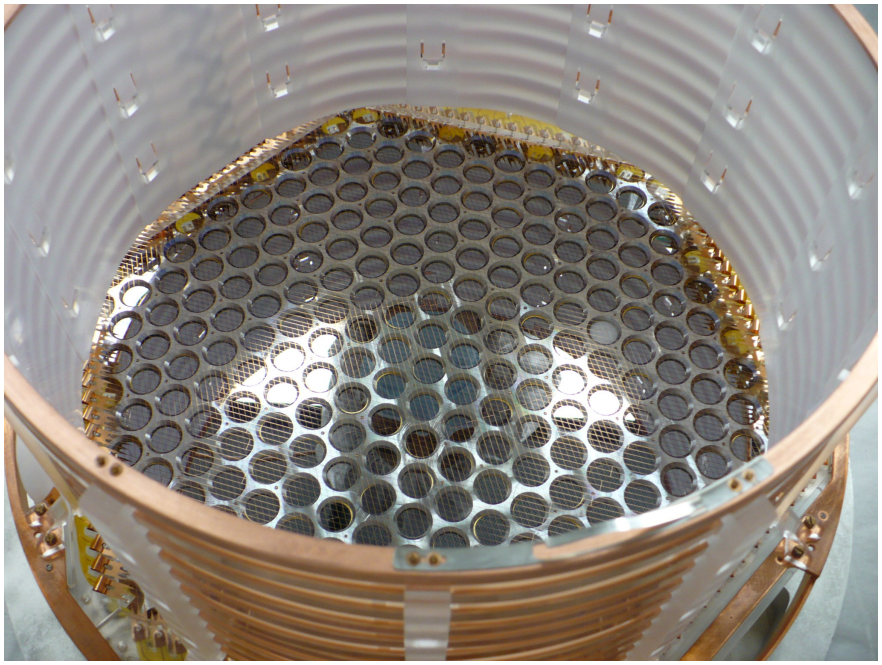

FIGURE 1.6. View of the detection plane in one of the two EXO-200 TPCs. [ref 0ν paper or whatev]

The cathode is set to 8 kV, providing an electric field of [xxx] V/cm across the 20 cm drift length of each TPC. Ionized electrons drift from the decay site, first passing the v-wires, which receive an induction signal, and are then collected by the u-wires, which are set at a 60° angle from the v-wires. The charge collection provides the remainder of the energy collection of the initial decay.

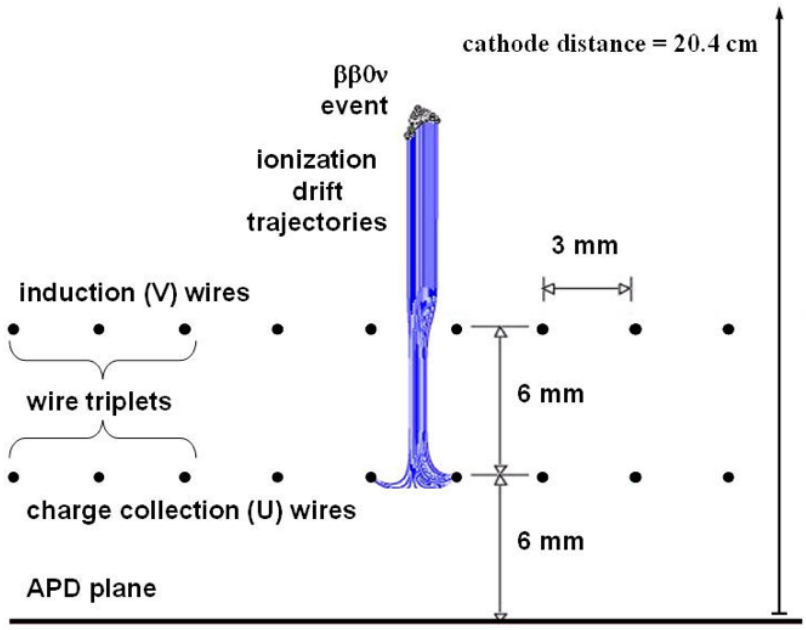

FIGURE 1.7. EXO-200 event detection.

Together, the u- and v-wires give an x/y position measurement for the event. The time between the initial scintillation detection and the charge collection give a z position, and a 3D position can be reconstructed for the event.

Having a reconstructed 3D event position is important in several ways. Firstly, position-based corrections on scintillation and charge collection can be applied. For charge, electronegative impurities in the LXe will absorb the drifting charge, requiring a drift-length (z-position) correction. High purity levels, measured in terms of electron lifetime, of [???] are maintained in EXO-200, but a small correction of [???] must still be applied [ref]. For scintillation, a full 3D correction is applied (called the Light Map), as some regions have more efficient light collection by the APDs [ref, maybe for whole paragraph].

A 3D position also allows a fiducial volume to be defined. The materials of the Teflon walls and cathode/detection planes contain more radioactive background-producing elements. Radioactive daughters from impurities like radon in the LXe bulk also tend to collect of the cathode [ref], so a stand-off distance of [???] is used as the fiducial cut.

Finally, 3D reconstruction allows the distinction between single-site (SS) and multi-site (MS) events. A(n?) MS event is one where two spatially separated events occur in the same [???]-μs time window. These are mostly caused by gamma rays interacting in the LXe, which can Compton-scatter several times. Rejecting MS events strongly separates gamma events from double beta decay events.

Of course, barium tagging will also require a 3D reconstructed position in nEXO.

Calibration of EXO-200 is done using various radioactive sources which can be moved to several positions around the outside of the TPC. Several different sources span the energy range of interest, but the main source is ^{228}Th, which produces gamma rays at [???] MeV, near the Q-value of ^{136}Xe double beta decay where the $0\nu\beta\beta$ peak will be. Source calibration data also provides a comparison between data and Monet-Carlo simulation, and provides the data for purity measurement and Light Map determination. Data and Monte-Carlo for ^{228}Th are shown in Fig. [ref fig source agreement].

The relationship between scintillation and ionization for a given event in LXe exhibits a well-known anti-correlation. Applying this to the combination of those signals improves the energy resolution, shown in Fig. [ref fig anticorrelation]. This correction defines a combined energy axis, called the rotated energy. Energy resolution is important in a $0\nu\beta\beta$ search, as it distinguished those events from $2\nu\beta\beta$ events in the tail of their spectrum. Resolution of [???] is achieved in [ref 0ν paper].

The final data set is fit using a combination of probability distribution functions (PDFs) for $0\nu\beta\beta$, $2\nu\beta\beta$, and all possible backgrounds. Fig. 1.8 shows the fits to the final energy spectrum data for (a) SS events, and (b) MS events. The green bands beneath each plot show the residuals vs. energy. The $2\nu\beta\beta$ spectrum, in gray, dominates the backgrounds in the SS spectrum. The red dotted lines in the SS spectrum outline the 2 σ region of interest around the Q-value, where the $0\nu\beta\beta$ peak will lie. The insets are a zoom into this region. The fit value for $0\nu\beta\beta$ in this dataset is non-zero, but it is not statistically significant enough to claim discovery [ref nature].

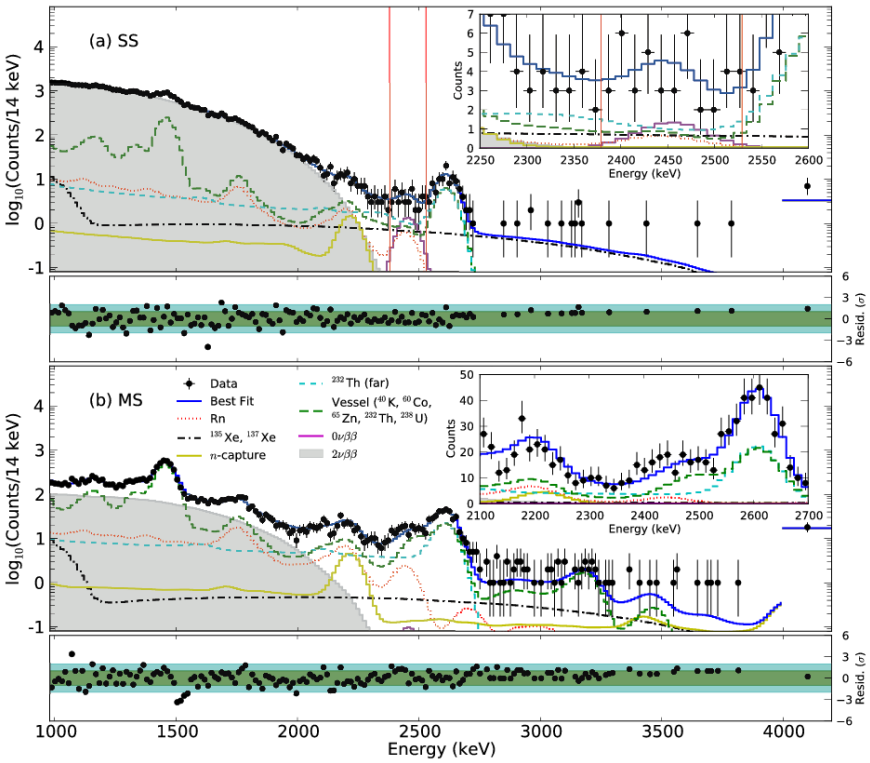

FIGURE 1.8. EXO-200 energy spectrum.

[ref nature] reports the most accurate measurement of the $2\nu\beta\beta$ of ^{136}Xe to date, at [???], and reports a limit on the half-life of $0\nu\beta\beta$ of ^{136}Xe of [???] at the 95 % confidence level,

which translates to an upper limit on the Majorana neutrino mass between [???] and [???], depending on the method of calculation for [which param?].

1.2.2. nEXO. The next-generation successor to EXO-200 is nEXO, a tonne-scale LXe TPC which will probe Majorana neutrino masses down to the [???] scale [ref]. The sensitivity projections for nEXO are shown in Fig. 1.9, along with those of EXO-200. nEXO will reach phase space where the two possible mass hierarchies begin to split; if nEXO successfully observes $0\nu\beta\beta$ in these regions, it may be able to also determine the mass hierarchy. Barium tagging will push the sensitivity further into the region allowed only by the normal hierarchy [ref for this?].

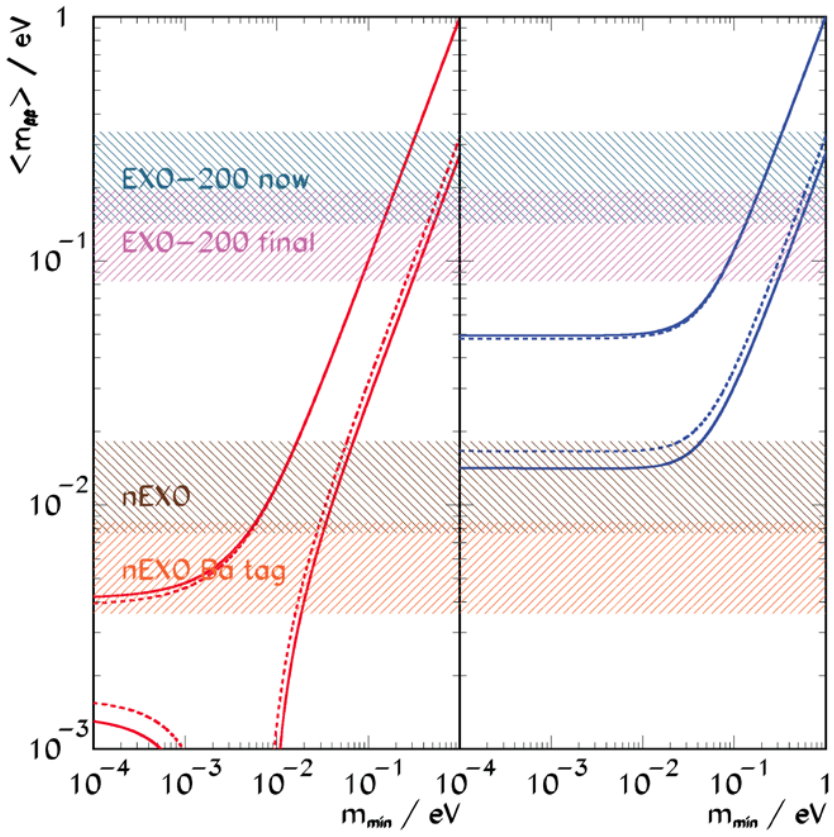

FIGURE 1.9. nEXO projected sensitivity to the Majorana neutrino mass vs. the sum of the three masses M_{total}. Is there an updated version? "To make this plot we used the best fit values of the mixing angles θsol=33.9, θatm=45, and θ13=0 and the Δm2s (Table I)" from review bb Rev...pdf (2008)

A schematic of the experimental setup is shown in Fig. 1.10 in one of the possible locations for nEXO, the SNOLAB cryopit. Similar to EXO-200, the copper-housed TPC will be submerged in HFE fluid, inside a copper cryostat. The cryostat will be insulated and submerged in a large volume of water shielding, in which photo-multiplier tubes could provide muon veto by observing Cherenkov radiation.

nEXO will be a single TPC with charge and light readouts at opposing ends of the TPC. Rather than wires, nEXO will use tile electrodes for charge readout, shown in Fig. 1.11.

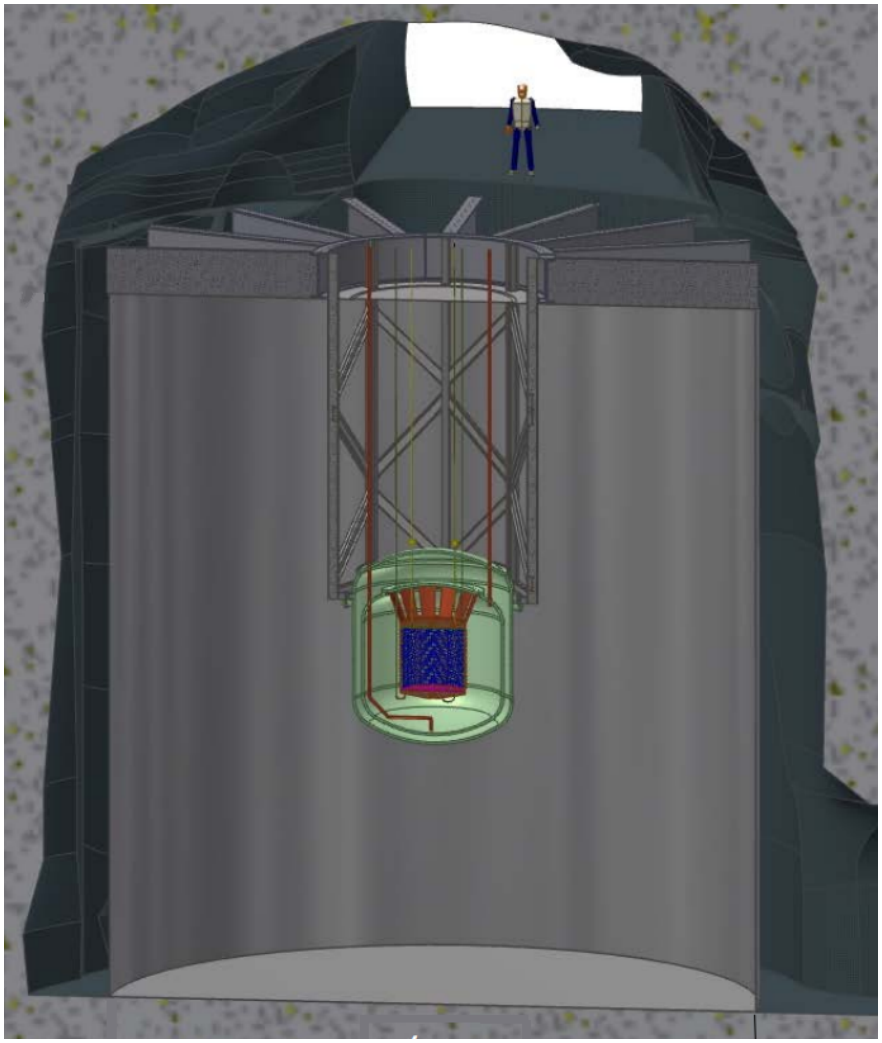

FIGURE 1.10. nEXO in the SNOLAB cryopit. Needs labels

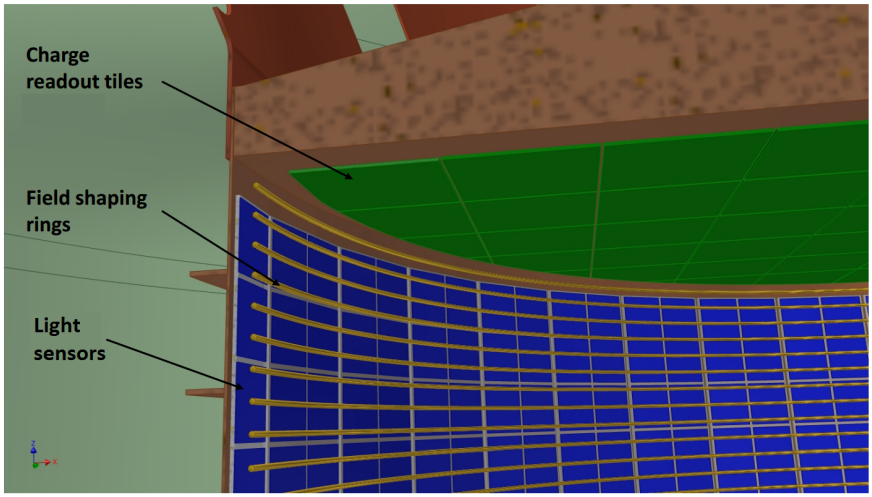

FIGURE 1.11. nEXO readout.

1.2.3. BARIUM TAGGING. The backgrounds observed around the Q-value in EXO-200 can be expected to scale up with the size of nEXO. But with the veto power of barium tagging, nEXO's sensitivity to $0\nu\beta\beta$ scales with the total ^{136}Xe mass in the detector, vs. the square root of that mass without barium tagging [ref].

Several possible barium tagging techniques have been proposed. Perhaps the most natural concept is to direct one or more lasers at the decay site to induce fluorescence of the barium daughter. This technique was explored thoroughly by Fairbank's group, and was abandoned when reliable fluorescence of Ba^+ in LXe could not be observed [ref Kendy's thesis].

Another concept was to grab the daughter in SXe on a cold probe, similar to the method explored in this thesis, but to then evaporate the SXe and drift the daughter into a trap for detection in vacuum. This method was abandoned when extraction of barium from SXe samples could not be achieved by Liang Yang's group [ref?].

Two barium tagging techniques continue to be explored. One of these is to grab the daughter on a surface, brought to the decay site by a probe, and then move it to a location where it can be desorbed from that surface by an infrared laser, and subsequently resonantly

ionized by two lasers in order to detect it by time-of-flight spectroscopy (or other trap/detect methods?). The apparatus for the study of this method is described in [instrumentation paper], along with some initial results.

The other remaining technique for barium tagging, now the concentration of Fairbank's group and the subject of this thesis, is what we call tagging in SXe. Here, we would send a cold probe to the site of the candidate $0\nu\beta\beta$ event in order to trap the Ba/Ba^+ in a small amount of SXe, and then observe it by its laser-induced fluorescence in the SXe, a technique called matrix isolation spectroscopy.

A concept for a probe is shown in Fig. [ref fig cryoprobe]. The SXe forms on a sapphire window or plug. Sapphire is a good candidate for a substrate; it has good thermal conductivity at low temperature, is extremely transparent, and can be purified to contain low amounts of fluorescing impurities such as Cr^{3+}. An excitation laser would be brought into the probe through a fiber, and aimed through the sapphire to excite the Ba/Ba^+ in the SXe. A return fiber could collect the laser reflections and used for measure the SXe thickness via interference fringes. **[in the fig., label things like the fibers like (A), (B), and just say what those are in the caption]** The Ba/Ba^+ fluorescence would then be collected by a lens/filter system and imaged onto a CCD. Additional components, not shown, would be required for cooling the sapphire, either by liquid He or by a Joule-Thompson nozzle, as well as a thermometer.

The next chapter describes theory relevant to single Ba/Ba^+ detection in SXe matrices.

CHAPTER 2

Theory

Theory relevant to the spectroscopy and detection of single Ba/Ba$^+$ in SXe matrices is discussed.

2.1. Ba/Ba$^+$ Spectroscopy in Vacuum

The lowest-lying energy levels in vacuum for Ba and Ba$^+$ are shown in Fig. 2.1. For Ba, the main transition is between the ground $6s^2\ {}^1S_0$ to the excited $6s6p\ {}^1P_1$ state. Spin(?)-suppressed transitions between the P state and three metastable D states results in a decay in to a D state after about 350 excitations. For Ba$^+$, two strong transitions exist between the ground $6s\ {}^2S_{1/2}$ **is the doublet correct??** and the $6p\ {}^2P_{1/2}$ and $6p\ {}^2P_{3/2}$ excited states. Transitions to the two metastable D states are higher than for the atom, resulting in a decay into a D state after about 4 excitations.

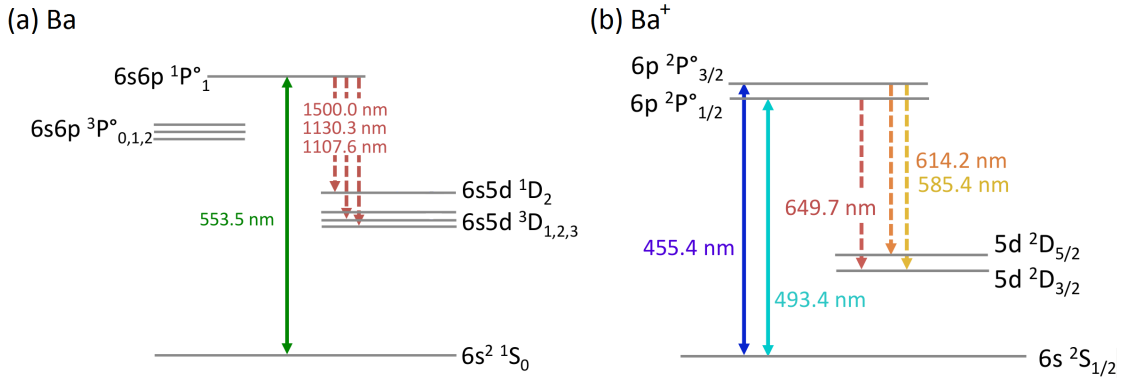

FIGURE 2.1. Energy level diagrams for (a) Ba and (b) Ba$^+$

These energy levels and their transition rates are well known, and are documented in the NIST tables [ref]. Single atom/ion detection by spectroscopy generally requires lasers to provide transitions out of the metastable D states once the atom/ion decays into one of them, in addition to the main excitation laser. For the atom, this requires three additional infrared

lasers, and single atom trapping/detection in a magneto-optical trap (MOT) is achieved in [ref Ba MOT]. Single Ba^+ observation requires only two lasers if the $^2P_{1/2}$ excited state is used. This is demonstrated in [ref something that does this ... is there something? How about the Carleton group?].

2.1.1. 5- or 6-level model? This could be for just the vacuum, and the in-matrix could reference it with changes (so I guess this would just be 5-level).

2.2. Matrix Isolation Spectroscopy

The spectroscopy of a species trapped in an inert solid matrix is called matrix isolation spectroscopy, the concept of which was pioneered around 19?? by [that one guy] [ref ... maybe [1] of ba spec]. Though absorption and emission are significantly broadened and shifted, a species can retain similarities to its vacuum counterpart, such as quantum numbers.

Studies of some matrix isolation systems have been made. The most thoroughly studied has been Na(?) in solid matrices of (Ar, Kr, Xe ?)... (Na? Mg?)...[refs]

We are of course interested in the spectroscopy of Ba and/or Ba^+ in SXe matrices, and this particular system has not been studied until recently. The first report of the spectroscopy of neutral Ba in SXe, along with candidate fluorescence peaks for Ba^+ in SXe, was published by our group in [ref ba spec], and conversations following this publication with ???'s group in ??? have confirmed our basic observations of the absorption spectrum of Ba in SXe.

From here forward I will refer to the host species as Xe and the guest as Ba/Ba^+, specific to our system. The leading interaction between [put this here if the van der waals is only necessarily the force for Ba in particular] the Ba/Ba^+ and a neighboring Xe atom is a (the) Van Der Waals (sp?) force, an induced dipole-dipole interaction. Xe is the most polarizable (sp?) of the noble gases.

The forms for this force(?) is shown in Eqn. [ref van der ba] for Ba and Eqn. [ref van der ba+] for Ba^+. Talk about it.

This binding between the Ba/Ba^+ and its surrounding Xe atoms results in vibrational modes, and the Franck Condon (sp?) principle applies. Fig. [ref fig franckcondon] helps illustrate this effect. In a cold matrix, the system will be in the ground vibrational state before excitation. The distribution of the wavefunction, even for the ground state alone, overlaps in space in general with more than one of the excited state vibrational modes, resulting in a broadening in energy of the absorption.

Rapid decay occurs to the lowest vibrational mode in the excited state before electronic decay can occur [ref] [is this just for Ba?]. Then a similar broadening in emission energy occurs as several overlapping vibrational mode wavefunctions exist in the ground electronic state, and a redshift is also observed as some energy was dissipated into phonons in the crystal in vibrational mode decays. **(How can you get a blueshift?)**

Shifts and broadening in absorption and emission depend in general on the distribution of Xe atoms around the Ba/Ba^+. The fcc crystal structure of the Xe restricts these environments to discrete number of so-called matrix sites, defined by (a) whether the Ba/Ba^+ is [intersituational or whatever – is that still a thing?], and (b) the number of vacancies in the Xe matrix surrounding the Ba/Ba^+. Experimental observation of emission peaks from different matrix sites of [Na] in solid noble gases is reported in [ref(s)], with theoretical calculations in [ref(s)] attributing observed peaks to specific vacancy distributions defining the matrix sites (maybe this has been done?).

Energy level transition probabilities can also be affected in a matrix. Distortions in electron wavefunction shapes by asymmetric matrix sites can affect radiative transitions by

altering parity [ref]. If electronic potential energy curves cross each other, nonradiative transitions can also become allowed for otherwise forbidden transitions [ref]. (Is a phonon emission called a nonradiative transition / does this actually happen?)

Jahn-Teller?

The detectability of a single atom/ion can depend greatly on altered transition rates. For example, in the Ba atom, matrix-allowed decay of the $^1P_1$ to the ^3P states could be much stronger than the main transition back to ground, which would suppress fluorescence and make single-atom detection impossible. But the matrix could also help by strengthening decays from the D states back to ground, eliminating any need for re-pump lasers to keep the transition cycle going.

CHAPTER 3

Apparatus

This chapter describes the apparatus at Colorado State University, which we have used for all described studies of Ba/Ba^+ fluorescence in SXe after deposition in vacuum. Our main barium source, the Ba^+ ion beam, is first described, as well as a purely Ba neutral source. The co-deposit of Ba/Ba^+ with Xe gas onto a cold sapphire window, subsequent laser excitation, and finally the collection optics for the fluorescence are described.

3.1. Ion Beam

The full ion beam is shown in Fig. 3.1. This is a clean source of Ba^+ which can do a very wide range of deposit sizes, from billions of ions in a focused laser region all the way down to the single-ion level , and even deposits sparse enough to scan a laser over spatially separated ions (may only want to say that if we have those scans).

3.1.1. Ion Source/Acceleration. Ba^+ ions are produced in a Colutron [type?] ion gun system [reference], shows Fig. [ref fig with ion source, showing Ar gas as well as Ba charge, and lens with ion path]. A solid barium charge is placed into the hollowed end of a stainless steel rod, which is then inserted into the discharge chamber, near the hot filament. The heated barium vaporizes, and is allowed to escape the hollowed rod around a loosely threaded set screw at the end of the rod.

The source is designed to produce a discharge between the anode plate and the filament cathode, through an argon buffer(?) gas leaked into the source chamber. This controlled discharge would then also ionize atoms, vaporized from the solid charge, to produce the desired ion beam, and Ar ions would be filtered out. However, to avoid contamination of

our solid matrix with residual Ar gas, we do not use the buffer gas in the ion source. We are still able to maintain a discharge between the filament and anode circuits. This discharge produces a plasma, containing barium ions, which escapes the chamber through a small hole in the anode, where it enters the acceleration potential.

The longevity of our ion current from a single charge (at least several 10s of hours) suggests that Ba is coating the inner walls of the chamber and is depleted slowly. This is supported by the observation of white oxidation of the inner source parts after a few minutes of exposure to air when opening the system.

The acceleration potential is 2 kV, between the ion source anode and an aperture, which is the first element of the Einzel lens 1. This lens approximately collimates the ion beam for passage through the E×B velocity filter.

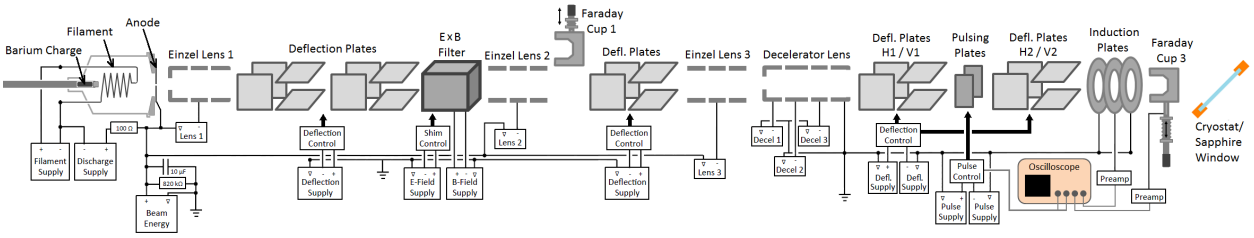

FIGURE 3.1. Ba^+ ion beam.

3.1.2. E×B VELOCITY FILTER. The E×B velocity filter selects Ba^+ by creating perpendicular electric and magnetic fields, which produce opposing forces on charged particles moving straight through the filter. The opposing forces will be equal for ions with velocity $v = \frac{E}{B}$. Since ion velocity is determined by mass (m), charge (q) and beam potential (V), the filter selects ions satisfying Eq. 4:

$$\frac{m}{q} = \frac{2VB^2}{E^2} \tag{4}$$

where B and E are the magnetic and electric fields, respectively. Those fields are chosen such that the forces are equal for Ba^+, while other ions will be deflected.

The E×B filter is shown in Fig. 3.2. Electromagnets provide the vertical magnetic field. Electrode plates and field-shaping guard rings provide the horizontal electric field. The guard rings prevent a lensing and astigmatism effect from fringe fields of the plates [8].

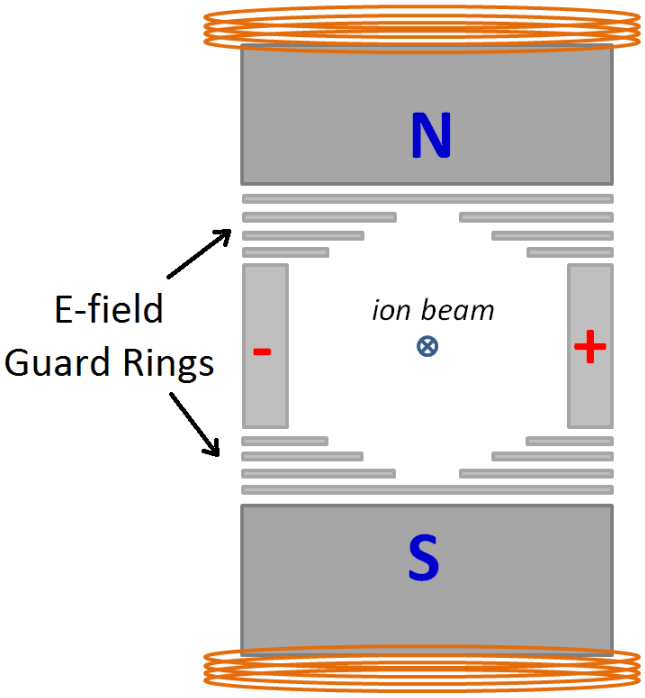

FIGURE 3.2. Colutron E×B ion velocity filter.

To determine the mass components of the beam, the electric field can be scanned. Fig. [ref mass scan fig] shows a scan of the Ba^+ beam, as well as of an Ar^+ beam. We found it necessary to run with the known mass of Ar in order to calibrate the magnetic field, which came to differ from the calculation given by Colutron [ref like Shon has?], likely due to hysteresis in the magnet. The Ba^+ peak agrees with the Ba mas s...

3.1.3. OTHER BEAM COMPONENTS. The first three sets of deflection plates can be used for beam diagnostics, and are set to 0 V during normal operation. The set just before the

pulsing plates, called H1 and V1, are set to constant values of 50 V and 0 V, respectively, which have been selected such that the beam, in both pulsing and continuous modes, can be deposited at the sapphire window for reasonable settings on the final deflection plates, H2 and V2. As described in 3.1.5, different settings in H2/V2 are required for peak ion current in cup 3 vs. peak deposit at the window.

Einzel lens 2 focuses the beam the pass through the aperture in the first element of the decelerator lens. Einzel lens 3 is not used in this setup. The decelerator lens can be used to vary Ba^+ deposit energy, but it in this work it acts as an Einzel lens with only the second element at voltage, and it focuses the beam at Faraday cup 3 (there is no Faraday cup 2 in this setup). Faraday cup 3 measures the ion current during experiments, and is retracted when deposits are being made. Its use in deposit calibration is described in 3.1.5. Faraday cup 1 is used for beam diagnostics, and is usually retracted on its bellows.

3.1.4. Ion Beam Pulsing. When running in pulsing mode, the pulsing plates are first set to 200 V and -200 V to deflect the beam, and are pulsed to 0 V for 2 μs for each pulse. The pulsing circuit is shown in Fig. [ref fig pulsing circuit, **ref Shon thesis if this is same figure**]. Square waves, triggered by LabVIEW at 50 Hz, enter the circuit at [x]. [describe how the pulse happens]

The induction plates observe pulses during a deposit. Pulses just prior to a deposit can be observed by cup 3 as well as the induction plates, for a local measurement of ion current in the pulses. An example of an oscilloscope readout of 16 averaged pulses is shown in Fig. [ref fig scope pulse – in caption, explain v-divided plate signals].

[x brand, or whatever] pre-amplifiers convert the ... [put this before scope picture?] [have a figure of the shaped plots too]

Pulsing data also provides additional confirmation that the beam is composed of Ba^+. [figure and data (**may need to *average* Ar+ as well as Ba+ stuff, w/ some kind of informed pulse data feature to determine velocity**) showing velocity measurement]

3.1.5. Calibration of Ion Deposit. To calibrate the signal at cup 3 to an ion density at the sapphire window, another Faraday cup (called cup w) is attached to the cold finger in place of the sapphire window. Firstly, the ratio in $\frac{fC}{pulse}$ between cup 3 and cup w is measured. Then, knowing the radius of cup w lets one determine the ion density per pulse at the sapphire window:

$$\frac{ions}{pulse \times m^2} = \frac{\sigma}{Ae} \tag{5}$$

where σ is

The required settings of the final deflection plates H2 and V2 are also determined by cup w. These typically differ from the peak values for cup 3 by about ???, corresponding to ??? mm.

Talk about beam size?

3.2. Ba Getter Source

Ba getters are neutral Ba sources typically used to grab reactive gas molecules in purifiers and vacuum tubes. We can use a getter as a source of neutral Ba. It is very helpful to have a completely different Ba source, especially a neutral-only source, in identifying observed fluorescence peaks. This is discussed further in 4.1.1.

The getter used briefly in this work is an endothermic ... getter wire ... [describe it] ... show diagram, maybe also of it in the system at same position as cup 3.

3.3. Solid Xenon Matrix Deposition

The final destination of the barium ions is of course in the solid xenon matrix, which is deposited onto a cold sapphire window. Sapphire has good thermal conductivity, good optical transparency in the visible, and does not fluorescese in the wavelength region where barium fluoresces.

Xenon freezes around 73 K (?) at our pressures (0.5 - 1 $\times$ 10^{-7} Torr ... it's lower when cold, can you determine what that is?), so the window is cooled to temperatures below that. The window is held to a cold finger (Fig. 6x, picture of), cooled by a -brand- cryostat.

3.3.1. Deposition Procedure.

Before barium ions are let through, xenon gas is allowed to flow, controlled by a leak valve, onto the cold sapphire window, where it freezes and begins growing the solid matrix. The Faraday cup is then retracted, to clear the path for barium ions. The cup serves as a shutter for DC deposition, or if pulsing is being used, they are performed at this time. Barium ions land in the solid xenon as the matrix continues to grow. The cup is then replaced, and the xenon leak stopped.

3.3.2. Laser Excitation.

3.3.3. Collection Optics.

talk about all that, including spectrometer

CHAPTER 4

Results

Improved studies of several emission peaks of neutral Ba in SXe, which are first reported in the theses of B. Mong [ref] and S. Cook [ref], are reported. The bleaching of several of these peaks is carefully observed (do a correction on p-meter sensitive area and on p-meter quantum efficiency, and also a spherical aberation correction for power??), and a model of atomic transition rates is fit to this data. Improved excitation spectra are achieved for all observed Ba emission peaks. Images of $\leq 10^{3?}$ Ba atoms are achieved using the bleaching peaks. Ultimately, images of Ba atoms at the few-atom level are achieved using the 619-nm fluorescence peak. Improved studies of candidate fluorescence peaks of Ba^+ in SXe are also reported. *Where/how should I reference the ba spec paper?*

4.1. Fluorescence of Ba in SXe

The multiple peaks observed from deposits of Ba in SXe are attributed to Ba atoms occupying different Xe matrix sites, the phenomena of which are described in Chapter 3 (*ref chap theory doesn't work*). Fig. [ref fig spectra for 10K, 50K, annealed 10K] shows spectra of Ba deposits under different conditions. A deposit made at 11 K shows a different ... um how is this described in the paper?

excitspec of 50 K [fig of all, including r110 of 619]... and 10 K?

leak rate dependence?

4.1.1. Identifying Peaks as Ba in SXe.

4.2. Bleaching

590 etc, model fit (see results intro paragraph)

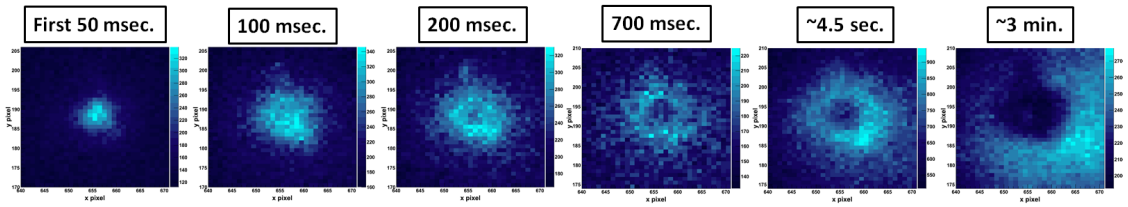

Figure 4.1

619, with the changes in time and I

4.3. Imaging

4.3.1. Imaging 577- and 591-nm peaks.

4.3.2. Imaging 619-nm peak.

CHAPTER 5

Conclusions

5.1. Future Steps

Talk about whatever Chris will do next ... ions? Other sites? Populations?

Talk about Adam's work, show pics and stuff.

Bibliography

[1] C.D. Ellis and W.A. Wooster, "The average energy of disintegration of radium e," *Proceedings of the Royal Society (London)* **A117** 109-123 (1927).

[2] F. Wilson, *American Journal of Physics* **36**, 12 (1968).

[3] K.A. Olive *et al.* (Particle Data Group), "14. Neutrino Mass, Mixing, and Oscillations," *Chin. Phys. C* **38**, 090001 (2014) (http://pdg.lbl.gov)

[4] B. Mong *et al.*, *Phys. Rev. A* **91**, 022505 (1954).

[5] K. Twelker *et al.*, *Review of Scientific Instruments* **85**, 095114 (2014).

[6] T. Brunner et al., *International Journal of Mass Spectrometry* **379** (2015) 110-120.

[7] M. Moe, *Phys. Rev. C* **44**, R931 (1991).

[8] L. W$\mathring{a}$hlin, "The Colutron, a Zero Deflection Isotope Separator," *Nuclear Instruments and Methods* **27** 55-60 (1964).